Influence of Turbulences and Cross-Wind on the Signal Quality in Circular Synthetic Aperture Radar

Michael Pircher[#1], Marc Jäger[#], Ulf Johannsen[*]
[#]Microwaves and Radar Institute, German Aerospace Center (DLR), Germany
[*]Electromagnetics Group, Eindhoven University of Technology, The Netherlands
[1]michael.pircher@dlr.de

***Abstract*— Airborne Circular Synthetic Aperture Radar (CSAR) measurements provide very high resolution, independent of the signal bandwidth. However, non-ideal flight conditions, such as turbulences or cross-wind, severely affect the coverage of the target area on the ground. The SNR of the received signal is reduced, and features in the image are more likely to be covered by noise. This paper analyzes these effects based on a flight campaign using the airborne F-SAR sensor of the German Aerospace Center (DLR), operating in C-band. It compares the results with an ideal steered antenna pattern, which mitigates the influence of turbulences. The ideal focused antenna pattern shows an improvement of 7.8 dB. The required beam steering angles for focusing the antenna footprint are presented as well, which potentially can be used to design future active phased array antennas, capable of compensating turbulences.**

***Keywords*— airborne radar, synthetic aperture radar, beam steering, phased arrays.**

I. INTRODUCTION

Airborne and spaceborne Synthetic Aperture Radar (SAR) systems play a crucial role, when it comes to geoscience and remote sensing. Independent on weather and daytime, they provide data about the Earth's surface dynamics, which are crucial for applications such as environmental monitoring, land cover classification or disaster response. Additionally SAR sees an increasing interest in monitoring the bio- and cryosphere. This includes for example soil moisture retrieval, forest height estimations, agricultural applications or glacier monitoring [1].

For long-term observations satellite SAR missions are used, since they provide constant monitoring of the Earth. Airborne systems have a shorter reaction time and a higher flexibility in their experimental setup. They can be deployed quickly or are often used as a testbed for new satellite SAR missions. The Microwaves and Radar Institute of the DLR operates an airborne SAR sensor, the F-SAR system, shown in Fig. 1. It allows fully polarimetric measurements in a frequency range starting from the P-band (350 MHz) to the X-band (9.6 GHz) [2].

Another advantage of airborne radar systems is their flexibility in terms of the flight path. They can perform SAR imaging modes, impossible for satellites, like Circular SAR (CSAR). The acquisition geometry is changed from a straight line to a circular trajectory as shown in Fig. 2. As the target area is illuminated from all directions, a sub-wavelength resolution can be achieved. In the ideal case of isotropic scatterers the resolution is $\lambda/4$ [3].

In airborne SAR the acquisition of the data can be affected substantially by turbulences and cross-wind, causing unwanted variation of the footprint on the ground. In case of CSAR it means that the observable area on the ground gets smaller because the footprints from all positions along the track don't fully overlap. The F-SAR system's fixed radiation pattern makes it unable to mitigate the effects of these temporal variations in the attitude angles.

This paper presents the influence of turbulences and cross-wind on the data acquisition in a typical CSAR flight. For an experimental analysis, a flight trajectory from a 2015 campaign over Wallerfing in Germany is shown and compared with the ideal focused results. The paper concludes with a presentation of the required beam steering angles. These finding could be used in the design for a future antenna, capable of electronic beam steering.

II. C-BAND ANTENNA SYSTEM OF F-SAR

The antennas of the F-SAR system (except for the P-band antenna) are placed in the antenna-carrier mounted on the starboard side of the airplane. Depending on the frequency the antennas are installed either at a certain inclination angle or parallel to the fuselage. In Fig. 1 the carrier and the antennas are shown, together with the antenna coordinate system. The antenna parameters were obtained in this coordinate system. The roll-axis of the airplane is parallel to the θ-axis of the antenna, and the yaw-axis is parallel to the ϕ-axis.

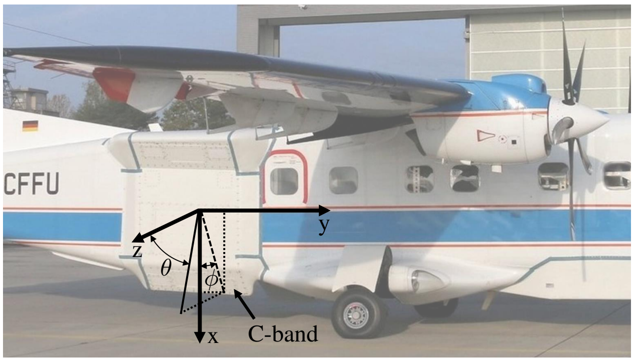

Fig. 1. The antenna carrier mounted at the airplane, with the C-band antenna and the antenna coordinate system.

In this study only the C-band antenna of the F-SAR system is considered. It consists of a rectangular array of 3 by 6 patch elements and has a length of 15.5 cm by 26.5 cm. The key characteristic of the antenna are:

- Center frequency: 5.3 GHz
- Bandwidth: 400 MHz
- Gain: 17 dBi in main beam direction
- Half-power beamwidth: 17° (ϕ) 23° (θ)
- Pointing: −3° (ϕ) 46° (θ)
- Sidelobe level: −17 dB
- Cross-polarization suppression: better than 25 dB

III. FLIGHT TRACK DATA SET

The considered circular flight trajectory was part of the Cropex-15 campaign conducted in 2015. Its aim was to investigate how the backscattering of crop fields changes with the seasons. It can be achieved by analyzing the backscattering properties of crop fields observed with various SAR imaging techniques, including different frequencies and polarization states. One part of Cropex-15 consists of a repeat pass interferometry measurement, in stripmap mode to achieve multiple baselines. This allows to resolve for scatterers along the height dimension, resulting in a tomographic SAR image [4].

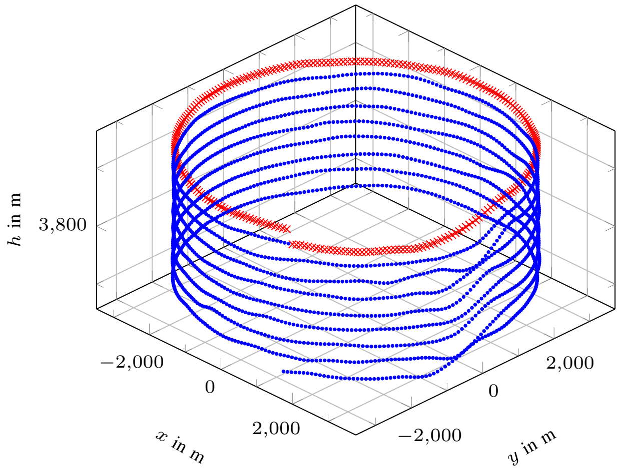

Fig. 2. Spiral flight track of the Cropex-15 mission, clearly showing the influence of turbulences, the red crosses indicate the flight track considered for the analysis in section V.

The second part was a spiral flight track, consisting of 9 windings. A SAR system in such an acquisition mode combines the advantages of the high resolution of CSAR with multiple baselines, providing full 3-D imaging with a very high resolution [4]. For this part of the mission C- and X-band data were acquired. The spiral measurement was conducted on July 10, 2015 under non-ideal flight conditions, namely cross-wind and turbulences.

All SAR acquisition flights are tracked by a Global Navigation Satellite System (GNSS) and an Inertial Measurement Unit (IMU), recording the position of the F-SAR system and the orientation of the airplane. In Fig. 2 the GNSS position of the sensor during the spiral flight is visualized, showing the influence of cross-wind. The first winding, marked in red crosses, is the data set used to compute the integrated backscatter power in section V.

The consequences of turbulences are twofold: The position does not follow the ideal trajectory, which needs to be corrected in the processing step, therefore the exact position of the sensor is needed. Not visible in Fig. 2 is the effect on the airplane's orientation. The IMU records the roll-, pitch- and yaw-angles of the airplane. On the one hand it allows to perform an antenna pattern calibration in the processing. On the other hand deviations from the ideal orientation of the sensor cause a significant jittering of the antenna footprint. The small beamwidth of the antenna in the ϕ-direction makes the deviations in the yaw-angle most critical.

IV. METHOD

In this section different metrics are presented, which can be used to describe the performance of SAR systems. The integrated backscatter power is used to evaluate the influence of turbulences in the previous discussed flight track. Therefore a software based simulation is developed, which is also presented in this section.

A. *NESZ and* P_{int}

A convenient way of describing the performance of SAR systems is the Noise-Equivalent Sigma Zero (NESZ). It is defined as the radar cross section of an area (σ_0), for which the Signal-to-Noise Ratio (SNR) is 1, corresponding to signal power equals noise power in the processed image. The NESZ can be derived by the system parameters as well as by analyzing the cross-polar channels of the final image. A high NESZ manifests itself in a reduced geometric and radiometric resolution of the processed image. Following the corresponding literature like [5] the formula for the NESZ can be derived as follows

$$\text{NESZ}(\theta,\phi) = \frac{2(4\pi)^3 r(\theta,\phi)^3 F_{\text{op}} \mathrm{k}_B T_{\text{s}} v}{P_{av} G(\theta,\phi)^2 \lambda^3 \delta_{\text{Gr}}}. \tag{1}$$

The quantities regarding noise are: F_{op} representing the operation noise factor, the Boltzmann constant k_B, and T_{s} stands for the noise temperature of the source. The distance from the sensor to the scatterer on the ground is denoted by $r(\theta,\phi)$ and v stands for the velocity of the SAR system. The average transmit power is represented by P_{av}, and $G(\theta,\phi)$ stands for the antenna gain. Let λ be the wavelength of the signal and δ_{Gr} the ground range pixel spacing.

The scope of this paper is to investigate the illumination of the target area on the ground. Since the formula for the NESZ in (1), includes different noise quantities, it is not well suited for this purpose, instead the integrated backscatter power is introduced, describing the power distribution over the ground, integrated along the synthetic aperture,

$$P_{\text{int}}(\theta,\phi) = \frac{P_{\text{av}} G^2(\theta,\phi) \lambda^3 \delta_{\text{Gr}} B_{\text{P}}}{2(4\pi)^3 r^3(\theta,\phi) v}. \tag{2}$$

The formula is obtained by approximating the noise bandwidth with the one sided bandwidth of the chirped radar pulse, B_P. Considering both (1) and (2), we see that all factors are system- or physical constants. Only the orientation of the antenna pattern ($G(\theta, \phi)$) and the distance to the ground ($r(\theta, \phi)$) are directly related to the acquisition geometry and the antenna pattern characteristics relevant for this study. Furthermore we see that $P_\mathrm{int}(\theta, \phi)$ is inversely proportional to the NESZ.

B. Simulation

A simulative approach is used to compute the integrated backscatter power, according to the following scheme. The GNSS position of the sensor is measured in the WGS84 coordinate system and for further processing the flight track is projected into the Universal Transverse Mercator (UTM) system, a Cartesian coordinate system [6]. The sensor's position with respect to the UTM system is denoted by $\vec{r}_\mathrm{sar} = (x_\mathrm{sar}, y_\mathrm{sar}, z_\mathrm{sar})^\mathrm{T}$.

In a first step, the illuminated area on the ground is discretized by sample points, spanning an equidistant grid of 4000 m by 4000 m. The sample points are defined in the UTM system, and are called $\vec{r}_\mathrm{sam} = (x_\mathrm{sam}, y_\mathrm{sam}, z_\mathrm{sam})^\mathrm{T}$. Considering both positions the difference vector $\vec{r}_\mathrm{diff} = \vec{r}_\mathrm{sam} - \vec{r}_\mathrm{sar}$ is calculated and $||\vec{r}_\mathrm{diff}||_2$ is the same as $r(\theta, \phi)$ in (1) and (2).

A third coordinate system is introduced to take account of the orientation of the airplane and the antenna. This is the antenna coordinate system, shown in Fig. 1. It considers the roll-, pitch-, and yaw-angles of the airplane as well as the mounting angle of the antenna carrier. A transformation of the $\vec{r}_\mathrm{sam}$ in the antenna coordinate system $\vec{r}_\mathrm{ant}$ allows the extraction of the θ and ϕ angles by

$$\theta = \arccos\left(\frac{r_{x,\mathrm{ant}}}{||\vec{r}_\mathrm{diff}||_2}\right) \tag{3}$$

and

$$\phi = \arctan\left(\frac{r_{y,\mathrm{ant}}}{r_{x,\mathrm{ant}}}\right). \tag{4}$$

The corresponding gain value $G(\theta, \phi)$ is found by interpolating the antenna pattern.

The previous steps allow the computation of the distance and the gain value for each sample point and sensor position pair. The backscatter power for each sample point is calculated by applying (2) and integrating over all sensor positions, to form P_int. This is done for all sample points on the ground. The result is a distribution of the integrated backscatter power projected on the ground, allowing a quantitative evaluation, which is presented in section V.

The same simulation is used to calculate the required beam steering angles, to compensate for the turbulences and focus the antenna pattern on a predefined point on the ground. It is transformed into the antenna coordinate system and by applying (3) and (4) the ideal pointing is calculated. Comparing with the actual pointing of the antenna leads to the required beam steering angle in ϕ and θ. The ideal pointing is also used to calculate the ideal integrated backscatter power.

For the calculation of the ideal P_int few assumptions are made: First, the electronic beam steering only affects the pointing of the main-beam, without influencing any other antenna characteristics such as gain or beamwidth. Secondly, the velocity has an influence on the NESZ as seen in (1). Since this effect can not be compensated by the antenna, it is neglected in the calculations.

V. RESULTS

In the following the results of the integrated backscatter power are presented. Several cases are investigated: First the simulation results are presented, obtained by the antenna having an ideal pointing, compensating for the turbulences. This ideal outcome is used for comparison with the results of the currently used fixed antenna. The section concludes with a discussion of the required beam steering angles to mitigate the turbulences.

A. Integrated Backscatter Power

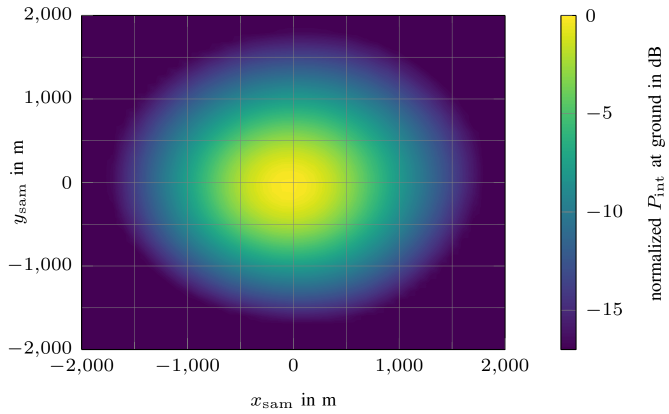

Fig. 3. The integrated backscatter power at the ground with the electronically steered, ideal pointing, using the red cross-marked flight track in Fig. 2.

The results shown in Fig. 3 are calculated by the algorithm presented in subsection IV-B. The antenna pointing is steered to the center of the scene, approximating the capabilities of an electronically scanned array. The maximum integrated backscattering power is normalized and the distribution on the ground is circularly symmetrical as expected. After 590 m the P_int decays by 50 %. The area on the ground within the 3 dB decay is $1.1\,\mathrm{km}^2$.

Fig. 4 shows the calculated P_int values on the ground for the currently used antenna. Since its pointing is fixed, the integrated backscatter power is smeared over a larger area. The values in Fig. 4 are normalized to the same factor as in Fig. 3, for comparison. The maximum value of P_int is about 7.8 dB lower than an ideal steered antenna. An unexpected result is the deviation of the maximum, which is not occurring at the center of the scene. It is shifted towards $x = 700\,\mathrm{m}, y = 500\,\mathrm{m}$, as a consequence of the strong cross-wind. The smearing makes it impossible to determine the half power decay.

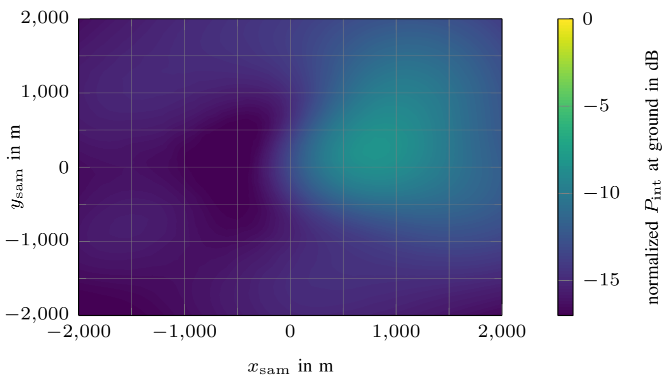

Fig. 4. The non-corrected integrated backscatter power at the ground, based on the red cross-marked flight track in Fig. 2.

B. *Beam Steering Angles*

The perfectly focused integrated backscatter power, like shown in Fig. 3, requires a steerable pointing of the antenna in both θ and ϕ. The data set of the spiral flight allows an individual analysis of 9 circular tracks, and the results are shown in Fig. 5 and Fig. 6. Dependent on the position of the airplane in the circle (indicated by the relative yaw-angle), a different beam steering angle is required. The blue curve shows the mean-value and the gray envelope covers the maximum values of all 9 tracks.

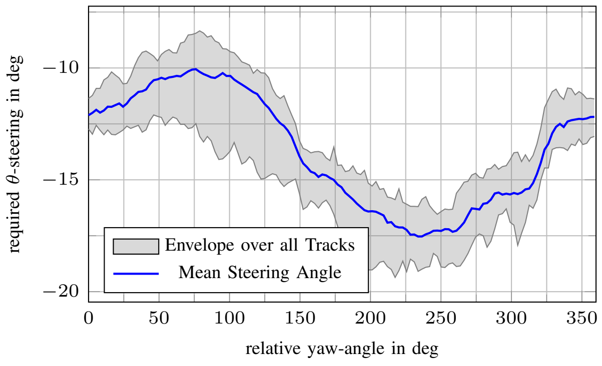

Fig. 5. Required beam-steering angle in θ over all tracks.

In the θ-dimension the required beam steering angle has to cover the range from −18.5° to −8.5°. The broad span of the envelope is caused by two effects: First, the spiral flight tracks require different steering angles as the altitude decreases and second, the turbulences. As the roll-axis is parallel to the θ-axis, the disturbance of turbulences is more distinctive.

In the ϕ-direction the beam needs to be steered over a larger range of at least ±13°. The small beamwidth of the antenna along ϕ requires a large steering angle. In Fig. 6 it can be seen, that the deviation of the tracks is very small. It behaves as expected, because the yaw-angle of the airplane, and therefore the ϕ-axis is more affected by the cross-wind and less by the turbulences.

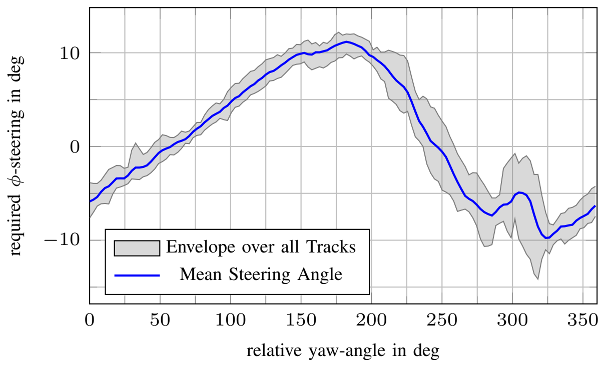

Fig. 6. Required beam-steering angle in ϕ over all tracks.

VI. CONCLUSION

In this work the influence of cross-wind and turbulences on the signal quality of CSAR is presented. For this purpose the integrated backscatter power is introduced. The analysis is based on a spiral flight track, obtained in 2015 and by considering the antenna pattern of the C-band antenna of DLR's F-SAR system.

The integrated backscatter power is calculated for two cases: First, for an antenna pattern ideally focused on a dedicated point on ground and second, for the real data with the fixed pointing. In the ideal focused case, the improvement of the integrated backscatter power is 7.8 dB. The beam-steering angles to focus the antenna pointing are calculated, showing that electronic beam steering is suitable to mitigate the influence of turbulences and cross-wind. The required range is ±13° in ϕ and between −18.5° and −8.5° in θ.

The investigation on how cross winds and turbulences affect the radiometric resolution is left for a future consideration.

ACKNOWLEDGMENT

Sincere gratitude is extended to Ralf Horn, for finding a proper data set and providing it. He works at the Microwaves and Radar Institute of the DLR.

REFERENCES

[1] A. Moreira, P. Prats-Iraola, M. Younis, G. Krieger, I. Hajnsek, and K. P. Papathanassiou, "A tutorial on synthetic aperture radar," *IEEE Geoscience and Remote Sensing Magazine*, vol. 1, no. 1, pp. 6–43, 2013.

[2] R. Horn, A. Nottensteiner, A. Reigber, J. Fischer, and R. Scheiber, "F-sar — dlr's new multifrequency polarimetric airborne sar," in *2009 IEEE International Geoscience and Remote Sensing Symposium*, vol. 2, 2009, pp. II-902–II-905.

[3] L. J. Moore and L. C. Potter, "Three-dimensional resolution for circular synthetic aperture radar," in *Proc. Algorithms Sythetic Aperture Radar Imagery IXV*, vol. 6568, 2007.

[4] A. Moreira et al., "Multi-baseline spaceborne sar imaging," in *2016 IEEE International Geoscience and Remote Sensing Symposium (IGARSS)*, 2016, pp. 1420–1423. DOI: 10.1109/IGARSS.2016.7729363.

[5] J. C. Curlander and R. N. McDonough, *Synthetic aperture radar systems and signal processing* (Wiley Series in Remote Sensing and Image Processing). Nashville, TN: John Wiley & Sons, 1991.

[6] *World geodetic system — 1984 (wgs-84) manual*, Second Edition, Doc 9674 AN/946, International Civil Aviation Organization (ICAO), Montreal, Canada, 2002.